Atmospheric Environment 181 (2018) 186–191

Contents lists available at ScienceDirect

Atmospheric Environment

journal homepage: www.elsevier.com/locate/atmosenv

Religious burning as a potential major source of atmospheric fine aerosols in summertime Lhasa on the Tibetan Plateau

Yu Yan Cui[a,b], Shang Liu[c,*], Zhixuan Bai[d,e], Jianchun Bian[d,f,**], Dan Li[d], Kaiyu Fan[d,g], Stuart A. McKeen[a,b], Laurel A. Watts[a,b], Steven J. Ciciora[b], Ru-Shan Gao[b]

[a] Cooperative Institute for Research in Environmental Sciences, University of Colorado, Boulder, CO, USA
[b] Chemical Sciences Division, NOAA Earth System Research Laboratory, Boulder, CO, USA
[c] School of Earth and Space Sciences, University of Science and Technology of China, Hefei, Anhui, China
[d] Key Laboratory of Middle Atmosphere and Global Environment Observation (LAGEO), Institute of Atmospheric Physics, Chinese Academy of Sciences, Beijing, China
[e] Shandong Provincial Key Laboratory of Ocean Environment Monitoring Technology, Institute of Oceanographic Instrumentation, Shandong Academy of Sciences, Qingdao, Shandong, China
[f] College of Earth Sciences, University of Chinese Academy of Sciences, Beijing, China
[g] Chengdu University of Information Technology, Chengdu, Sichuan, China

GRAPHICAL ABSTRACT

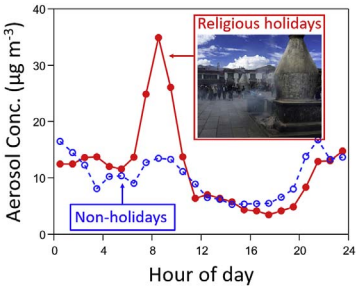

ARTICLE INFO

Keywords:
Tibetan Plateau
Aerosol size distribution
Religious activities
Incense burning
Biomass burning
Source apportionment

ABSTRACT

We carried out field measurements of aerosols in Lhasa, a major city in the Tibetan Plateau that has been experiencing fast urbanization and industrialization. Aerosol number size distribution was continuously measured using an optical particle size spectrometer near the center of Lhasa city during the Asian summer monsoon season in 2016. The mass concentration of fine particles was modulated by boundary layer dynamics, with an average of 11 $\mu g\,m^{-3}$ and the high values exceeding 50 $\mu g\,m^{-3}$ during religious holidays. Daytime high concentration coincided with the religious burning of biomass and incense in the temples during morning hours, which produced heavy smoke. Factor analysis revealed a factor that likely represented religious burning. The factor contributed 34% of the campaign-average fine particle mass and the contribution reached up to 80% during religious holidays. The mass size distribution of aerosols produced from religious burnings peaked at ~500 nm, indicating that these particles could efficiently decrease visibility and promote health risk. Because of its significance, our results suggest that further studies of religious burning, a currently under-studied source, are

* Corresponding author.
** Corresponding author. Key Laboratory of Middle Atmosphere and Global Environment Observation (LAGEO), Institute of Atmospheric Physics, Chinese Academy of Sciences, Beijing, China.
E-mail addresses: shangliu@ustc.edu.cn (S. Liu), bjc@mail.iap.ac.cn (J. Bian).

https://doi.org/10.1016/j.atmosenv.2018.03.025
Received 4 September 2017; Received in revised form 20 February 2018; Accepted 11 March 2018
Available online 12 March 2018

needed in the Tibetan Plateau and in other regions of the world where religious burnings are frequently practiced.

1. Introduction

The Tibetan Plateau (TP), the largest and highest highland in the world, plays a key role in regional climate in Central and East Asia (Kutzbach et al., 1993; Wu et al., 2012). The TP is generally considered as a pristine environment and background region for atmospheric aerosols (Cong et al., 2007; Liu et al., 2017). Concerns have been raised that the rapid increase of anthropogenic emissions in Asia may influence the air quality in the TP region (Cong et al., 2007). Measurements of air pollutants in the TP, however, are scant because of the high altitude and harsh climate.

Lhasa is the capital of the Tibet Autonomous Region of China, as well as the economic and cultural center of the TP. The city has experienced fast urbanization and economic growth during the past decades (Gong et al., 2011). As the hub of Tibetan Buddhism, Lhasa has been attracting thousands of visitors each year, making tourism the pillar of the city's GDP. As a result, the 63 km^2 urban area of Lhasa city hosts ~0.4 million floating population, which doubles the ~0.2 million local residents estimated for year 2012 (Ran et al., 2014). The thriving tourism has boosted the energy consumption, construction projects, and religious burning activities that can deteriorate the city's air quality. In addition, Lhasa city lies in the Lhasa River Valley (Fig. 1). The mountain range surrounding the Lhasa city prevents efficient diffusion of air pollutants. Moreover, incomplete fuel combustion resulting from the low oxygen concentration in the Lhasa (3.6 km above sea level) atmosphere may amplify the extent of air pollution in the city (Bishop et al., 2001; Wang et al., 2010). The high solar radiation can further enhance photochemistry and thus the production of secondary pollution, such as ozone and secondary organic aerosols (Norsang et al., 2009; Ran et al., 2014). Overall, the remoteness, high elevation, increased combustion emissions, and unfavorable topography make Lhasa a unique site for the air quality research.

Aerosol measurements in Lhasa are extremely limited. Most of the studies investigated the elemental composition of aerosols, either through single-particle (Duo et al., 2015; Zhang et al., 2000, 2001a) or bulk sample analysis (Cong et al., 2011; Zhang et al., 2001b). Others focused on particle-bound organochlorine (Li et al., 2008) or polycyclic aromatic hydrocarbons (PAHs; Liu et al., 2013). Huang et al. (2010) separated the fossil and non-fossil fractions of carbon in total suspended particles (TSP) using ^{14}C measurements. They found that non-fossil carbon (likely included biomass burning and biogenic aerosols) contributed ~40% of total carbon to TSP in summer, which is consistent with previous studies implying that biomass burning could be an important source in Lhasa (Duo et al., 2015; Zhang et al., 2001b). However, the source apportionment of total aerosol mass, especially for fine aerosols, have not been conducted to the best of our knowledge.

In this work, we studied the aerosol size distribution in Lhasa city. The size distribution of fine aerosols was continuously measured with a high-sensitivity optical particle counter for a ~three-week period, followed by source identification using factor analysis. Special attention was given to the aerosols generated from religious burnings, which have not been extensively studied in the air quality research community (Lung et al., 2003).

2. Experimental methods

2.1. Instrumentation and model simulation

The ground-based sampling site was located at the China Reference Climatological Station of Lhasa in the downtown area (29.66° N, 91.14° E), which is 3.6 km above sea level. The station occupies approximately 25,000 m^2 open space with a suite of instruments situating on the ground. The ground is covered by lawn. There are no tall buildings surrounding the station. Our instrument was located near the center of the station, with an inlet height of 1.5 m above ground level. Particle number size distribution was continuously measured using a custom-built optical particle sensor, the Printed Optical Particle Spectrometer (POPS) in the period of 2–20 August 2016 during the Asian summer monsoon. The POPS is a single particle counter that records the pulse information produced by each particle passing through a 405 nm laser beam (Gao et al., 2016). The performance of the POPS instrument has been carefully established using standard calibration material and validated via inter-comparison with other accepted instruments (e.g. UHSAS and LAS, Gao et al., 2016). Its scientific usefulness has been demonstrated by recent field studies (Telg et al., 2017; Yu et al., 2017). Particle size is calculated from the calibration curve, which relates the pulse height to the size of the particle. The calibration curve was derived by introducing a series of size-selected particles to the POPS instrument. The size-selected particles were generated by atomizing solution of dioctyl sebacate (DOS) followed by sizing with a differential mobility analyzer. Therefore, the reported particle size in this paper is DOS-equivalent diameter. The size calibration was further checked using commercial polystyrene latex spheres. The mass of each detected particle was calculated using its retrieved size, assuming that the particles are spherical and have a constant density of 1.6 g cm^{-3}. The measured particles were binned logarithmically into 14 size bins across the POPS detection range (140– 3 000 nm) with ΔlogDp of 0.1, except for the last bin with a smaller ΔlogDp of 0.03 because of the upper detection limit of 3 000 nm. The aerosol mass for each size (ΔM) bin was calculated as the sum of all individual particle mass in the size bin. ΔM values were normalized by their respective ΔlogDp to derive the particle mass size distribution, expressed as dM/dlogDp. The ensemble particle mass was calculated as the sum of the mass of all measured particles. The data were averaged to 10-min intervals for in-depth analysis.

The planetary boundary layer (PBL) height was measured using the meteorological operational GTS1 radiosonde (Bian et al., 2011) carried into the atmosphere by weather balloons. Three balloons were launched daily in the morning (7:15), around noon (13:15), and in the evening (19:15) during the sampling period. We note that Tibet Autonomous Region uses Beijing Time, which is ~1.9 h earlier than the apparent solar time in Tibet. Beijing time (local time) is used throughout the text. The PBL height was determined by vertical profile of the virtual potential temperature (θ_v). Under the nocturnal stable

Fig. 1. Topographic map of Lhasa City. The star indicates the sampling site.

boundary conditions, the low-level jet was also analyzed to assist the PBL height determination.

In addition to the measurements, we used the Weather Research and Forecasting (WRF) model v3.8.1 to simulate the meteorological variables (Skamarock et al., 2008). The model domain has 410 × 360 horizontal grid cells with a 12 km spatial resolution, and 51 vertical layers from surface to 50 hpa. WRF simulations were performed for 1–22 August. Each simulation was integrated by 30 h with the first 6 h being spin-up time. Global Forecast System/National Centers for Environmental Prediction (GFS/NCEP) data were used to provide initial and boundary conditions for the simulation. The following physics schemes were used for the WRF simulation: the Monin–Obukhov scheme for the surface layer, the Yonsei University (YSU) scheme (Hong and Noh, 2006) for the planetary boundary layer, the Noah Land Surface Model (Chen and Dudhia, 2001) for land parameterization, the Rapid Radiative Transfer Model (Mlawer et al., 1997) for the long-wave and short-wave radiation, the Kain–Fritsch scheme (Kain, 2004) for the cumulus parameterization, and the WRF single moment 3-class microphysics scheme (Hong et al., 2004) for the microphysical parameterization. The bulk Richardson number method (Hong and Pan, 1996) was used to obtain the diagnostic PBL height. The modeled PBL height generally agrees with the PBL height derived from the radiosonde measurements (Fig. 2, Fig. S1), with the modeled morning PBL height slightly lower than observation.

We used residence time analysis of the Lagrangian particle dispersion model FLEXible PARTicle-Weather Research and Forecasting (FLEXPART-WRF; Ashbaugh et al., 1985; Brioude et al., 2013; de Foy et al., 2015; Stohl et al., 2005) to show the spatial pattern of transport to the sampling site. Four-day back-trajectories were generated for each hourly sample using FLEXPART-WRF with a 12 × 12 km spatial resolution. The back-trajectories in Fig. S2 show the origin of air masses arriving at the sampling site from the surface to 10 km.

2.2. Receptor modeling

Positive matrix factorization (PMF2) was applied to the particle mass size distribution to identify the sources that contributed to the particle mass. The PMF method was developed by Paatero and Tapper (1994) and has been widely used in the air quality research community (Liu et al., 2016; Ulbrich et al., 2009; Zhang et al., 2011). PMF decomposes the measured matrix into linearly-independent components. The components can then be linked to specific source types by their characteristic profiles and/or comparison of their time series with those of the external tracers (Zhang et al., 2011).

The input data matrix was composed of the time series of the mass of the 14 size bins. Several factors were considered to estimate the error for each data point in the input data matrix in preparation for the input error matrix. First, the uncertainty in particle counting is calculated as the square root of the particle count rate. This is suitable because the particle counting measurement follows Poisson distribution, in which the uncertainty equals the square root of the particle count (de Gouw et al., 2003; Hayward et al., 2002; Liu et al., 2016). Additional factors include the uncertainty in the flow rate (10%) and the uncertainty in the assumed particle density (10%). These uncertainties were propagated using error propagation rules to calculate the final error for each data point. The robust mode of PMF was used, in which the influence of the outliers (normalized errors > 4) was reduced during the fitting process. The rotational parameter FPEAK values of ± 1, ± 0.8, ± 0.6, ± 0.4, ± 0.2, and 0 were examined, which resulted in nearly identical factors. The plot of $Q/Q_{expected}$ as a function of FPEAK value, a theoretical diagnostic for the PMF solutions (Ulbrich et al., 2009), showed a "U" shape, with FPEAK = 0 corresponding to the minimum $Q/Q_{expected}$ (Fig. S3a). Therefore, the results from FPEAK = 0 were selected as the optimal solution. Seed values of 0–100 (varied by 10) were examined. The effect of seeds on the results was negligible, supporting the robustness of the solution.

PMF solutions of two to five factors were investigated. The two-factor solution fit poorly to the time series and missed some peaks completely. Using three, four, and five factors produced two robust factors (factors 2 and 3 in Fig. 3). Using factors greater than three simply splits factor 1 in Fig. 3, resulting in physically unrealistic factor profiles. Therefore the three-factor solution was selected as the final result. In this solution, the $Q/Q_{expected}$ value was 1.05 (Fig. S3b), close to 1 for the idealized solution. The distribution of scaled residuals for the bins centers around 0 and approximately Gaussian (Fig. S4), suggesting that the data are well fit and the residuals represent random noise. The uncertainty of the selected factors was evaluated using bootstrapping analysis (100 runs). The average 1-σ uncertainties for the factor time series and factor profile were 3% and 7% (Fig. S5), respectively, supporting the robustness of the PMF solution.

3. Results and discussion

3.1. Meteorological conditions and origin of air masses

The sampling period was characterized by mostly sunny days, except for August 7 and 13 during which light rain occurred. The air temperature ranged from 9 °C to 24 °C, with the lows and highs occurring at ~5:00 and ~17:00, respectively. Relative humidity anti-correlated with air temperature, with a campaign-average value of 54% (Fig. S6).

The PBL height showed a consistent diurnal pattern. Low PBL height (< 200 m above ground level) was observed during nighttime and early morning hours. The PBL height started to increase at 8:00 and reached its maximum (~2000 m above ground level) at 16:00. The dramatic PBL height increase during the afternoon indicates that the particle concentration was significantly diluted by a factor of 10 or more compared to the morning concentrations.

The air mass footprints produced using the FLEXPART-WRF model show that the air masses mainly originated from the south and southeast region of Lhasa (Fig. S2), suggesting that the contribution of natural dust from the deserts in Northern and Northwestern China was small. This is consistent with previous study demonstrating that local sources control the air pollution in Lhasa (Duo et al., 2015).

3.2. Mass size distribution of fine particles

The estimated campaign-average mass concentration was 11 ± 2.2 μg m^{-3} for particles with diameters of 140–3 000 nm, which was ~half of the $PM_{2.5}$ concentration (25 μg m^{-3}) in wintertime Lhasa (Duo et al., 2015). The concentration was higher than other remote regions in the TP that are not as populated as in Lhasa (e.g., the TSP

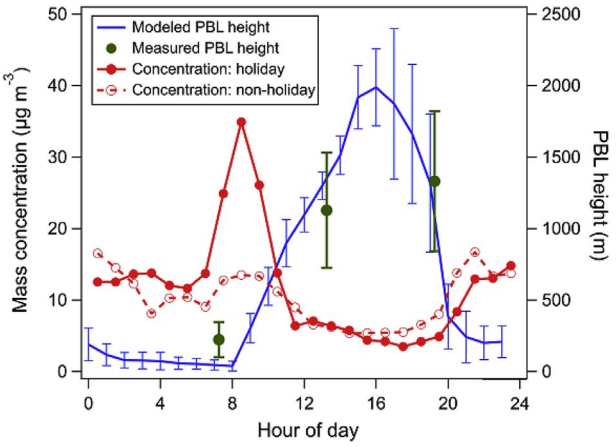

Fig. 2. Diurnal cycle of particle mass concentration for holidays and non-holidays, modeled PBL height, and measured PBL height above ground level.

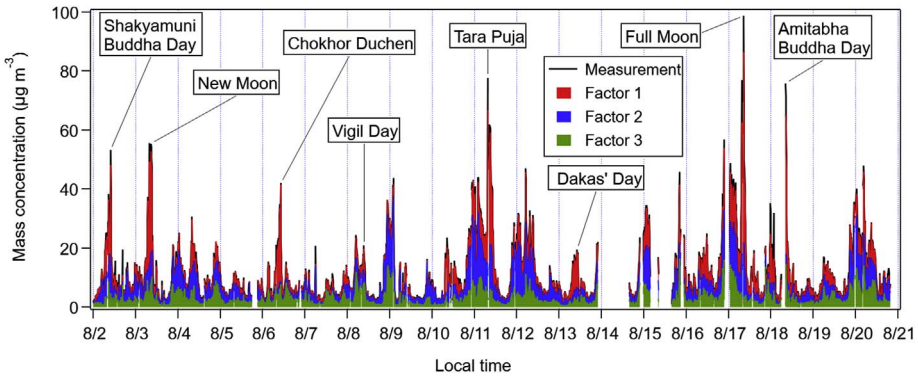

Fig. 3. Time series of particle mass concentration divided into factor 1 (the religious burning factor), factor 2 (the dust factor), and factor 3 (the fossil fuel combustion/secondary factor). The days with major religious activities are labeled. Linear correlation of the reconstructed and the measured particle mass results in r^2 of 0.99 and a slope of 0.95 (Fig. S7).

concentration in Nam Co was ~1.5 μg m^{-3} in August of 2007; Cong et al., 2009), but was substantially smaller than that in summertime Beijing (~70 μg m^{-3}), Shanghai (~40 μg m^{-3}), and Guangzhou (~30 μg m^{-3}), the major polluted cities in China (Zhang and Cao, 2015). In addition, the mass concentration in Lhasa was lower than the $PM_{2.5}$ concentration in other high-altitude urban areas (> 3 000 m a.s.l.), e.g., the $PM_{2.5}$ concentration in Puno and Cusco in Peru was reported to be 23 μg m^{-3} and 41.3 μg m^{-3}, respectively (Pearce et al., 2009; Pollard et al., 2014). As a reference, the national ambient air quality standards of China require that the annual mean concentration of $PM_{2.5}$ in Chinese cities does not exceed 35 μg m^{-3} (Cao et al., 2013). The diurnal cycle of the mass concentration showed highs at night and in the early morning and lows in the afternoon, anticorrelating with the PBL height (Fig. 2), suggesting that the PBL dynamics played a key role in modulating the particle pollution.

Episodes with daytime high particulate pollution (> 40 μg m^{-3}) were observed on August 2, 3, 6, 11, 17, and 18 (Fig. 3). During these events, the particle number and mass concentration started to increase rapidly at ~6:00, reached peak value at ~9:00, and then decreased quickly till noon (Fig. 2). These pollution episodes largely coincided with religious events/holidays on August 2, 3, 6, 8, 11, 13, 17, and 18 (http://www.wheeloftheyear.com/2016/buddhist.htm, last accessed on 3/15/2018; Fig. 3), during which substantial burning activities occurred in and around the temples near downtown Lhasa and possibly in suburban residential areas. Two exceptions were observed on August 8 and 13, in which days the particle concentration was relatively low compared to the concentration in other holidays. Wet removal of particles was likely responsible for the low concentration on August 13. The cause of the low concentration on August 8 was unclear.

3.3. Sources of fine particles

Significant difference in particle mass size distribution was observed between holiday and non-holiday days (Fig. 4). The total particle mass concentration during holidays was about twice as high as that during non-holiday days, reflecting the influence of burning activities on particle concentration. A distinct accumulation mode centering at ~500 nm in the mass size distribution was observed in holidays but not in non-holidays. This mode is typical for the mass size distribution of biomass and incense burning aerosols (Fang et al., 2002; Janhäll et al., 2010; Seinfeld and Pandis, 2006).

The PMF analysis resulted in three factors. The factor time series are shown in Fig. 3, and the mass size distribution and diurnal variation are shown in Fig. 5.

The high peaks observed in the time series of total particle mass (Fig. 3) were extracted as a single factor, suggesting a unique source for the pollution episodes. The peaks in the time series of the factor coincided with the timing of the religious burning activities. For this reason, the first factor was identified as a religious burning factor. The factor profile (Fig. 5a) resembled the difference of the mass size distribution between holiday and non-holiday days as shown in Fig. 4b (r = 0.93), which features a peak mode at 440–560 nm. Previous studies have reported that the mass size distribution of aerosols emitted from incense burning generally have a peak at ~300–600 nm (Fang et al., 2002; Jetter et al., 2002; Ji et al., 2010; Yang et al., 2007). For example, Fang et al. (2002) and Yang et al. (2007) showed that the peak in the mass size distribution of incense burning aerosols occurred at 320–560 nm. The consistency of the peak accumulation mode in the factor profile with the literature results further supports that the factor could represent religious burning, a common activity during the Tibetan religious ceremony.

The profile of the second factor showed a major peak at ~3 μm (Fig. 5b). This factor may represent dust particles, which are typically in the coarse mode (Zender et al., 2003). As the contribution of long-range transported dust to Lhasa air was minimal (Fig. S2), the dust particles observed in this study likely originated from wind and traffic

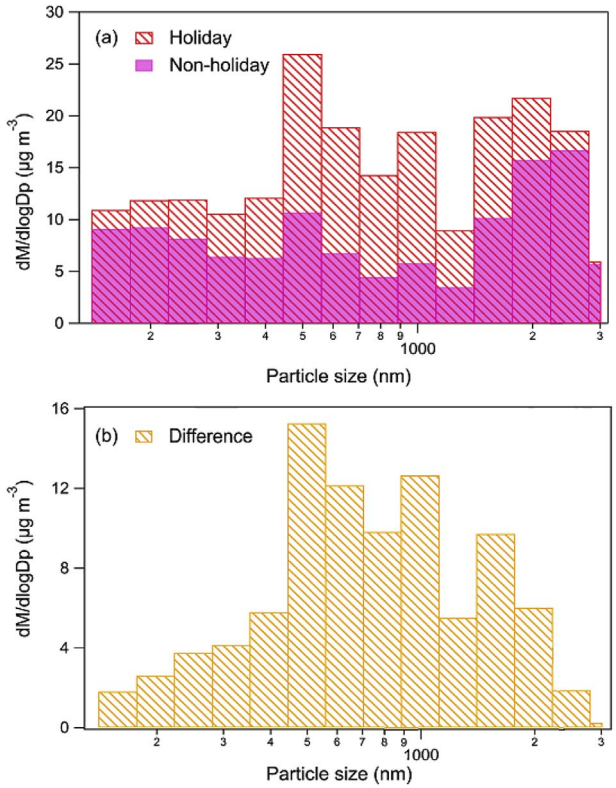

Fig. 4. (a) Comparison of the mass size distribution of holiday and non-holiday days. (b) The difference of mass size distribution between holiday and non-holiday days.

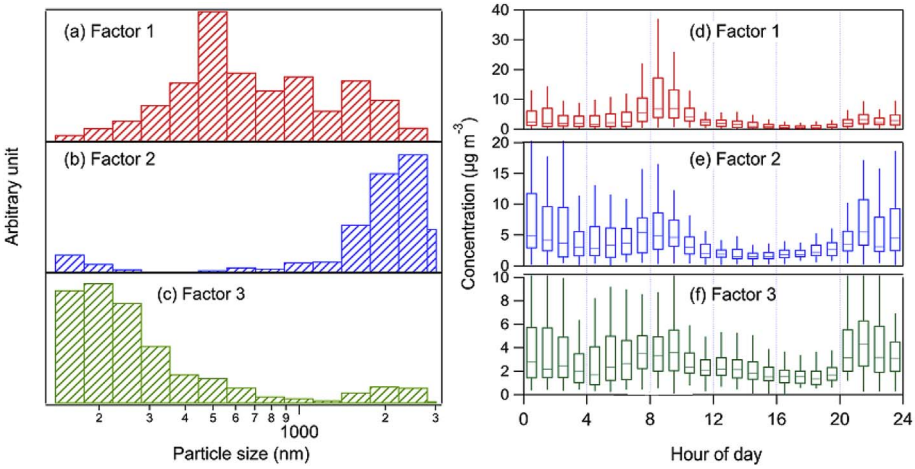

Fig. 5. Factor profile (a)–(c) and diurnal variation (d)–(f) for the factors identified from the PMF analysis.

induced suspension of local road dusts. The factor also contained 4% mass for particles smaller than 300 nm, which may be because of primary particles emitted from traffic exhaust that were mixed with suspended dusts. Another possibility would be the incomplete separation of this factor with the other factors. In this case, an uncertainty of 4% would be added to the factor mass concentration, which was insignificant. The second factor was identified as a road dust factor.

The third factor was dominated by small particles (200 nm; Fig. 5c), which could represent fresh emissions from fossil fuel combustion and/or secondarily formed particles. The factor profile was similar to the mass size distribution of aerosols emitted from motor vehicles (Kleeman et al., 2000), which was dominated by a fine mode. The factor concentration showed a morning peak at 8:00–9:00, which is typical of vehicular emissions. There was an evening maximum starting at 19:00 and peaked at 22:00. This maximum may result from a combination of low PBL height (Fig. 2) and emissions from the trucks used for building construction, which was observed to occur during both day and night throughout the study. The factor was termed as a fossil fuel combustion (FFC)/secondary factor.

3.4. Contribution of religious burnings

The religious burning factor, the road dust factor, and the FFC/secondary factors contributed 34%, 38%, and 28% of the campaign-average particle mass, respectively. In particular, the contribution of the religious burning factor reached up to ~80% during religious holidays, suggesting that this source could significantly impair the air quality in Lhasa. Religious combustion in Lhasa mainly includes incense (Dowman, 2008) and biomass burning (Duo et al., 2015). Burning of biomass in large burners outside of the temples or households is called Weisang, a traditional and widespread custom in Tibet. A wide variety of materials can be used for burning, including branches of pine and cypress, wormwood, and other herbs and heather leaves. Both biomass and incense burnings emit large amount of carcinogenic PAHs (Jetter et al., 2002; Simoneit, 2002), expose to which could induce health problems (Chiang and Liao, 2006). Numerous temples exist in the Lhasa city. None of these temples is immediately next to our sampling site. Even though our observations were made at a fixed location, the religious burning factor extracted from our data should be representative for large city areas that are not adjacent to temples.

4. Conclusions

In summary, we observed high aerosol pollution episodes in summertime Lhasa, which were likely generated by religious burning activities. The burning contributed to one third of the total fine particle mass during the measurement period and about 80% during religious holidays, thereby significantly reduced the air quality during the period. As Tibet has become more accessible and increasingly attractive to tourists from around the world, the contribution from religious burnings is likely to increase. The heavy burning smokes could promote exposure risk of fine particulates and the toxic components in them, especially for the temple workers. Co-emitted gas-phase organics, coupled with NO_x emission from cars and trucks and high UV flux can lead to high O_3 production. This pilot study draws attention to further investigate the chemical and physical properties of pollutants from religious burning activities, which could help constrain their impacts on air quality and human health.

Acknowledgements

We thank Dr. Michael Trainer (NOAA-Earth System Research Laboratory) for helpful discussions. The field campaign was funded by the National Science Foundation of China (91337214 and 41675040) and Key Research Program of Frontier Sciences of CAS (QYZDY-SSW-DQC027) and the NOAA Climate Program Office. S. L. acknowledges the support from National Science Foundation of China (21777151). We are grateful for NOAA's High Performance Computing Program for their support in running WRF and FLEXPART models.

Appendix A. Supplementary data

Supplementary data related to this article can be found at http://dx.doi.org/10.1016/j.atmosenv.2018.03.025.

References

Ashbaugh, L.L., Malm, W.C., Sadeh, W.Z., 1985. A residence time probability analysis of sulfur concentrations at grand-canyon- national-park. Atmos. Environ. 19, 1263–1270.
Bian, J., Chen, H., Vomel, H., Duan, Y., Xuan, Y., Lu, D., 2011. Intercomparison of humidity and temperature sensors: GTS1, Vaisala RS80, and CFH. Adv. Atmos. Sci. 28, 139–146.
Bishop, G.A., Morris, J.A., Stedman, D.H., Cohen, L.H., Countess, R.J., Countess, S.J., Maly, P., Scherer, S., 2001. The effects of altitude on heavy-duty diesel truck on-road emissions. Environ. Sci. Technol. 35, 1574–1578.
Brioude, J., Arnold, D., Stohl, A., Cassiani, M., Morton, D., Seibert, P., Angevine, W., Evan, S., Dingwell, A., Fast, J.D., Easter, R.C., Pisso, I., Burkhart, J., Wotawa, G., 2013. The Lagrangian particle dispersion model FLEXPART-WRF version 3.1. Geosci. Model Dev. (GMD) 6, 1889–1904.
Cao, J., Chow, J.C., Lee, F.S.C., Watson, J.G., 2013. Evolution of PM2.5 measurements and standards in the U.S. and future perspectives for China. Aerosol Air Qual. Res. 13, 1197–1211.
Chen, F., Dudhia, J., 2001. Coupling an advanced land surface–hydrology model with the Penn State–NCAR MM5 modeling system. Part I: model implementation and sensitivity. Mon. Weather Rev. 129, 569–585.
Chiang, K.C., Liao, C.M., 2006. Heavy incense burning in temples promotes exposure risk

from airborne PMs and carcinogenic PAHs. Sci. Total Environ. 372, 64–75.
Cong, Z., Kang, S., Liu, X., Wang, G., 2007. Elemental composition of aerosol in the Nam Co region, Tibetan Plateau, during summer monsoon season. Atmos. Environ. 41, 1180–1187.
Cong, Z., Kang, S., Dong, S., Zhang, Y., 2009. Individual particle analysis of atmospheric aerosols at Nam Co, Tibetan Plateau. Aerosol Air Qual. Res. 9, 323–331.
Cong, Z., Kang, S., Luo, C., Li, Q., Huang, J., Gao, S., Li, X., 2011. Trace elements and lead isotopic composition of PM10 in Lhasa, Tibet. Atmos. Environ. 45, 6210–6215.
Dowman, K., 2008. The Power-places of Central Tibet: the Pilgrim's Guide. Routledge & Kegan Paul, London and New York.
Duo, B., Zhang, Y., Kong, L., Fu, H., Hu, Y., Chen, J., Li, L., Qiong, A., 2015. Individual particle analysis of aerosols collected at Lhasa City in the Tibetan Plateau. J. Environ. Sci. 29, 165–177.
Fang, G.C., Chu, C.C., Wu, Y.S., Fu, P.C., 2002. Emission characters of particulate concentrations and dry deposition studies for incense burning at a Taiwanese temple. Toxicol. Ind. Health 18, 183–190.
de Foy, B., Cui, Y.Y., Schauer, J.J., Janssen, M., Turner, J.R., Wiedinmyer, C., 2015. Estimating sources of elemental and organic carbon and their temporal emission patterns using a least squares inverse model and hourly measurements from the St. Louis–Midwest supersite. Atmos. Chem. Phys. 15, 2405–2427.
Gao, R.S., Telg, H., Mclaughlin, R.J., Ciciora, S.J., Watts, L.A., Richardson, M.S., Schwarz, J.P., Perring, A.E., Thornberry, T.D., Rollins, A.W., Markovic, M.Z., Johnson, J.E., Fahey, D.W., Telg, H., Mclaughlin, R.J., Ciciora, S.J., Watts, L.A., Richardson, M.S., 2016. A light-weight, high-sensitivity particle spectrometer for PM2.5 aerosol measurements. Aerosol Sci. Technol. 6826, 88–99.
Gong, P., Wang, X., Yao, T., 2011. Ambient distribution of particulate- and gas-phase n-alkanes and polycyclic aromatic hydrocarbons in the Tibetan Plateau. Environ. Earth Sci. 64, 1703–1711.
de Gouw, J. a., Goldan, P.D., Warneke, C., Kuster, W.C., Roberts, J.M., Marchewka, M., Bertman, S.B., Pszenny, A.A.P., Keene, W.C., 2003. Validation of proton transfer reaction-mass spectrometry (PTR-MS) measurements of gas-phase organic compounds in the atmosphere during the New England Air Quality Study (NEAQS) in 2002. J. Geophys. Res. 108. http://dx.doi.org/10.1029/2003JD003863.
Hayward, S., Hewitt, C., Sartin, J.H., Owen, S.M., 2002. Performance characteristics of a proton transfer reaction-mass spectrometer for measuring volatile organic compounds in ambient air. Environ. Sci. Technol. 36, 1554–1560.
Hong, S.-Y., Noh, Y., 2006. A new vertical diffusion package with an explicit treatment of entrainment processes. Mon. Weather Rev. 134, 2318–2341.
Hong, S.Y., Pan, H.L., 1996. Nonlocal boundary layer vertical diffusion in a medium-range forecase model. Mon. Weather Rev. 124, 2322–2339.
Hong, S.Y., Dudhia, J., Chen, S.H., 2004. A revised approach to ice-microphysical processes for the bulk parameteriza-tion of cloud and precipitation. Mon. Weather Rev. 132, 103–120.
Huang, J., Kang, S., Shen, C., Cong, Z., Liu, K., Wang, W., Liu, L., 2010. Seasonal variations and sources of ambient fossil and biogenic-derived carbonaceous aerosols based on 14C measurements in Lhasa, Tibet. Atmos. Res. 96, 553–559.
Janhäll, S., Andreae, M.O., Pöschl, U., 2010. Biomass burning aerosol emissions from vegetation fires: particle number and mass emission factors and size distributions. Atmos. Chem. Phys. 10, 1427–1439.
Jetter, J.J., Guo, Z., McBrian, J.A., Flynn, M.R., 2002. Characterization of emissions from burning incense. Sci. Total Environ. 295, 51–67.
Ji, X., Bihan, O.L., Ramalho, O., Mandin, C., D'Anna, B., Martinon, L., Nicolas, M., Bard, D., Pairon, J.C., 2010. Characterization of particles emitted by incense burning in an experimental house. Indoor Air 20, 147–158.
Kain, J.S., 2004. The Kain–Fritsch convective parameterization: an update. J. Appl. Meteorol. 43, 170–181.
Kleeman, M.J., Schauer, J.J., Cass, G.R., 2000. Size and composition distribution of fine particulate matter emitted from motor vehicles. Environ. Sci. Technol. 34, 1132–1142.
Kutzbach, J.E., Prell, W.L., Ruddiman, W.F., 1993. Sensitivity of Eurasian climate to surface uplift of the Tibetan Plateau. J. Geol. 101, 177–190.
Li, J., Lin, T., Qi, S., Zhang, G., Liu, X., Li, K., 2008. Evidence of local emission of organochlorine pesticides in the Tibetan plateau. Atmos. Environ. 42, 7397–7404.
Liu, B., Cong, Z., Wang, Y., Xin, J., Wan, X., Pan, Y., Liu, Z., Wang, Y., Zhang, G., Wang, Z., Wang, Y., Kang, S., 2017. Background aerosol over the Himalayas and Tibetan Plateau: observed characteristics of aerosol mass loading. Atmos. Chem. Phys. 17, 449–463.
Liu, J., Li, J., Lin, T., Liu, D., Xu, Y., Chaemfa, C., Qi, S., Liu, F., Zhang, G., 2013. Diurnal and nocturnal variations of PAHs in the Lhasa atmosphere, Tibetan Plateau: implication for local sources and the impact of atmospheric degradation processing. Atmos. Res. 124, 34–43.
Liu, S., Li, R., Wild, R.J., Warneke, C., de Gouw, J.A., Brown, S.S., Miller, S.L., Luongo, J.C., Jimenez, J.L., Ziemann, P.J., 2016. Contribution of human-related sources to indoor volatile organic compounds in a university classroom. Indoor Air 26, 925–938.
Lung, S.C.C., Kao, M.C., Hu, S.C., 2003. Contribution of incense burning to indoor PM10 and particle-bound polycyclic aromatic hydrocarbons under two ventilation conditions. Indoor Air 13, 194–199.
Mlawer, E.J., Taubman, S.J., Brown, P.D., Iacono, M.J., Clough, S.A., 1997. Radiative transfer for inhomogeneous atmospheres: RRTM, a validated correlated-k model for the longwave. J. Geophys. Res. 102, 16663–16682.
Norsang, G., Kocbach, L., Tsoja, W., Stamnes, J.J., Dahlback, A., Nema, P., 2009. Ground-based measurements and modeling of solar UV-B radiation in Lhasa, Tibet. Atmos. Environ. 43, 1498–1502.
Paatero, P., Tapper, U., 1994. Positive matrix factorization: a non-negative factor model with optimal utilization of error estimates of data values. Environmentrics 5, 111–126.
Pearce, J.L., Rathbun, S.L., Aguilar-Villalobos, M., Naeher, L.P., 2009. Characterizing the spatiotemporal variability of PM2.5 in Cusco, Peru using kriging with external drift. Atmos. Environ. 43, 2060–2069.
Pollard, S.L., Williams, D.L., Breysse, P.N., Baron, P.A., Grajeda, L.M., Gilman, R.H., Miranda, J.J., Checkley, W., CRONICAS Cohort Study Group, 2014. Environ. Health 13. http://dx.doi.org/10.1186/1476-069X-13-21.
Ran, L., Lin, W.L., Deji, Y.Z., La, B., Tsering, P.M., Xu, X.B., Wang, W., 2014. Surface gas pollutants in Lhasa, a highland city of Tibet – current levels and pollution implications. Atmos. Chem. Phys. 14, 10721–10730.
Seinfeld, J., Pandis, S., 2006. Atmospheric Chemistry and Physics: from Air Pollution to Climate Change. Wiley, Hoboken, N. J.
Simoneit, B.R.T., 2002. Biomass burning - a review of organic tracers for smoke from incomplete combustion. Appl. Geochem. 129–162.
Skamarock, W.C., Klemp, J.B., Dudhia, J., Gill, D.O., Barker, D.M., Duda, M.G., Huang, X.Y., Wang, W., Powers, J.G., 2008. A description of the advanced research WRF version 3. NCAR Tech. http://dx.doi.org/10.5065/D68S4MVH. Note NCAR/TN-475+STR.
Stohl, A., Forster, C., Frank, A., Seibert, P., Wotawa, G., 2005. Technical note: the Lagrangian particle dispersion model FLEXPART version 6.2. Atmos. Chem. Phys. 5, 2461–2474.
Telg, H., Murphy, D.M., Bates, T.S., Johnson, J.E., Quinn, P.K., Giardi, F., Gao, R.S., 2017. A practical set of miniaturized instruments for vertical profiling of aerosol physical properties. Aerosol Sci. Technol. 51. http://dx.doi.org/10.1080/02786826.2017.1296103.
Ulbrich, I.M., Canagaratna, M.R., Zhang, Q., Worsnop, D.R., Jimenez, J.L., 2009. Interpretation of organic components from positive matrix factorization of aerosol mass spectrometric data. Atmos. Chem. Phys. 9, 2891–2918.
Wang, Y., Yang, L., Zhou, X., Dai, J., Zhou, Y., Deng, Z., 2010. Experiment study of the altitude effects on spontaneous ignition characteristics of wood. Fuel 89, 1029–1034.
Wu, G.X., Liu, Y.M., He, B., Bao, Q., Duan, A.M., Jin, F.F., 2012. Thermal controls on the Asian summer monsoon. Sci. Rep. 2, 404.
Yang, C.R., Lin, T.C., Chang, F.H., 2007. Particle size distribution and PAH concentrations of incense smoke in a combustion chamber. Environ. Pollut. 145, 606–615.
Yu, P., Rosenlof, K.H., Liu, S., Telg, H., Thornberry, T.D., Rollins, A.W., Portmann, R.W., Bai, Z., Ray, E.A., Duan, Y., Pan, L.L., Toon, O.B., Bian, J., Gao, R.S., 2017. Efficient transport of tropospheric aerosol into the stratosphere via the Asian summer monsoon anticyclone. Proc. Nat. Acad. Sci. USA 114, 6972–6977.
Zender, C.S., Bian, H., Newman, D., 2003. Mineral Dust Entrainment And Deposition (DEAD) model: description and 1990s dust climatology. J. Geophys. Res. Atmos. 108. http://dx.doi.org/10.1029/2002JD002775.
Zhang, D., Iwasaka, Y., Bai, Y., Shi, G., 2000. Aerosol particles around Lhasa city, Tibet, China, in summer 1998: individual particle analysis. J. Aerosol Sci. 31, 319–320.
Zhang, D., Iwasaka, Y., Shi, G., 2001a. Soot particles and their impacts on the mass cycle in the Tibetan atmosphere. Atmos. Environ. 35, 5883–5894.
Zhang, Q., Jimenez, J.L., Canagaratna, M.R., Ulbrich, I.M., Ng, N.L., Worsnop, D.R., Sun, Y., 2011. Understanding atmospheric organic aerosols via factor analysis of aerosol mass spectrometry: a review. Anal. Bioanal. Chem. 401, 3045–3067.
Zhang, X.Y., Arimoto, R., Cao, J.J., An, Z.S., Wang, D., 2001b. Atmospheric dust aerosol over the Tibetan Plateau. J. Geophys. Res. Atmos. 106. http://dx.doi.org/10.1029/2000JD900672.
Zhang, Y.-L., Cao, F., 2015. Fine particulate matter (PM2.5) in China at a city level. Sci. Rep. 5. http://dx.doi.org/10.1038/srep14884.